Contents lists available at Science-Gate

International Journal of Advanced and Applied Sciences

Journal homepage: https://www.science-gate.com/IJAAS.html

Prediction of large-scale earthquakes using precursor earthquakes: A regression study

Yu-Fan Fu, Zhong-Wei Zhang, Xin-Yue Yang, Shu Yuan *

College of Resources, Sichuan Agricultural University, Chengdu 611130, China

ARTICLE INFO

Article history:
Received 22 April 2025
Received in revised form
5 January 2026
Accepted 27 February 2026

Keywords:
Earthquake prediction
Triggering earthquakes
Triggered earthquakes
Regression model
Seismology

ABSTRACT

Earthquake prediction remains a major challenge in seismology, and no reliable method has yet been established. Previous studies suggest that large earthquakes (triggered earthquakes, TDEs) are often preceded by smaller events (triggering earthquakes, TGEs), but their quantitative relationship is unclear. In this study, we developed a prediction method based on four quadratic regression equations linking magnitude and distance between TGEs and TDEs, and three linear regression equations linking magnitude and time interval. The method was tested on 87 large earthquakes (M ≥ 6.6) from the past 100 years, including the 2023 Turkey (M7.8) and 2025 Myanmar (M7.7) events. Results show that 89% of epicenters and 63% of occurrence times were successfully predicted. For earthquakes of M ≥ 9.0 and those causing major casualties, the model achieved an accuracy within 100 km and 3 days, outperforming most existing approaches. Based on these results, we also propose a prediction for a future earthquake in Japan.

1. Introduction

Earthquakes have a large impact on human life. Large earthquakes that happen in a densely populated area may cause the deaths of more than thousands of people. However, earthquake prediction is a very difficult problem, and so far, there is no reliable prediction model (Rundle et al., 2002; Kerr, 2011; Denolle et al., 2014; Hall, 2023). Some earthquake-prone countries have established early warning systems, the main principle of which is to monitor the pressure wave (P-wave) emitted from the earthquake's epicenter and to send a warning before the destructive shear wave (S-wave) arrives. Because the time interval between the two types of waves is generally not more than 30 seconds, the practical use of this type of early warning system is very limited (Cyranoski, 2004). Recently, Bletery and Nocquet (2023) presented a systematic analysis of changes in the horizontal position of approximately 3000 geodetic stations and found that horizontal movements of these stations exponentially accelerated in a direction consistent with slow fault slip near the eventual earthquake nucleation point in the last 2 hours before the earthquake ruptures. Thus, an hour-level early warning system might be built.

Studies of earthquake precursors have mainly included research on seismic statistics, crustal deformation, gravity, geomagnetic field, geoelectrical properties, hydro geochemistry, underground fluid dynamics, stress and strain, meteorological, interferometric synthetic aperture radar (InSAR) interferometry, and thermal infrared radiation (TIR) abnormality (Cisternas et al., 2005; Friedmann, 2012; Tramutoli et al., 2013; Eleftheriou et al., 2016; Moro et al., 2017). Among the proposed theories about the origin, the abrupt release of greenhouse gas (e.g., CO_2 and CH_4) has been suggested to explain the emergence of anomalous TIR signals in some correlations with the time and the place of earthquake occurrence (Tramutoli et al., 2013; Eleftheriou et al., 2016). Wei et al. (2013) found significant thermal radiation anomalies before and after earthquakes of magnitude (M) ≥ 7.0. Thermal radiation with abnormal duration, range, and morphology is closely related to the geological structure. Yue et al. (2022) further extracted pre-seismic anomaly from multi-channel TIR remote sensing images and indicated that the successful prediction rate from 4-channel anomalies was 41.94%, which was much higher than that of one-channel anomalies with the same distance range of 200 km. Ionospheric total electron content (TEC) anomalies have been found to have occurred 8 hours

* Corresponding Author.
Email Address: roundtree318@hotmail.com (S. Yuan)
https://doi.org/10.21833/ijaas.2026.03.003
Corresponding author's ORCID profile:
https://orcid.org/0000-0001-6565-6914

before the Philippines earthquake (*M*7.6 on August 31, 2012), but these precursors may not always be detectable before every large-scale earthquake (Lin, 2013). Han et al. (2022) found that the atmospherically electric-field data obtained from the calculation were found to be in good concordance with the detected data of the Wenchuan (China) *M*7.9 earthquake, implying that the atmospherically electric-field anomalies may be used as earthquake precursors. However, the accuracy of earthquake prediction using these precursors still needs to be verified, and in most cases, convincing evidence with theoretical models is still lacking.

Among previous studies, the theory of the harmonic oscillation wave driven by the tidal force (HT wave) is particularly interesting. A method of impending earthquake prediction using HT waves was proposed by Qian et al. (2009). HT waves primarily appear a few days before the main shock. These HT waves may be a type of wave propagating along the pore fluid in porous crustal rocks in an acoustic mode, and therefore, they can be monitored by measuring the changes in the georesistivity. According to the time difference between the arrival of the P-wave and that of the S-wave, the distance between the station and the epicenter of the future earthquake can be determined. Qian et al. (2009) used this model to successfully predict the Wenchuan (China) *M*7.9 earthquake. Based on the RT wave model, we proposed a prediction method by analyzing the associations between the major earthquakes and the surrounding slightly smaller earthquakes, and achieved a certain success rate. However, direct evidence of HT waves is still lacking, and it is hard to prove.

The region-time-length (RTL) algorithm has been widely used for investigating precursory seismicity changes before large and moderate earthquakes (Gambino et al., 2014). Recently, machine learning methods, e.g., decision tree (DT), shallow neural network (SNN) with the contemporary deep neural network (DNN), long short-term memory (LSTM) neural networks, gated recurrent network (GRU), support vector machine (SVM), or random forest to identify patterns in meta-databases have been proposed to improve earthquake forecasting (Yousefzadeh et al., 2021; Berhich et al., 2022; Klyuev et al., 2022). Wang et al. (2023) suggested that some small earthquakes contain information related to a possible future large earthquake, and machine learning methods provide a promising avenue for improving the forecasting of large-scale earthquakes. A new list of earthquake catalogs has been developed through supervising machine-learning results with unprecedented detail. Using unsupervised machine learning methods to analyze complex data of seismicity might be a feasible way to improve earthquake prediction performance (Beroza et al., 2021; Herrera et al., 2022; Mousavi and Beroza, 2022; Zhang et al., 2022; Mousavi and Beroza, 2023; Dascher-Cousineau et al., 2023; Liu et al., 2023a).

Coupling between triggering earthquake (TGE) and triggered earthquake (TDE) has been well documented (Cisternas et al., 2005; Liu et al., 2023b). Earthquakes could be triggered by local alternations in the stress field (static triggering), by the adjacent earthquakes, or by the stress induced by the passage of a surface (Rayleigh and Love) wave from a far-away but large-scale earthquake (dynamic triggering) (Velasco et al., 2008). Although only about 2–3% of global main shocks could cause remote triggering in each region (Parsons et al., 2014), in our previous study, we found that large earthquakes of magnitude ≥ 7 were generally associated with several precursor earthquakes of magnitude ≥ 5.6. However, no quantitative relation was proposed previously. Here, we further indicate that the associations could be described by several regression equations. Based on the regression equations, a novel prediction method was proposed. We further investigated large-scale earthquakes over the past 100 years and found that 63%–89% of them fit the model, and the forecasting accuracy achieved 100 km and 3 days. Strengths and weaknesses of our prediction method were further discussed by comparing with other prediction strategies, especially the machine learning methods. The research is very similar to the problem-solving approach, which is an old metric. However, different from previous studies, our algorithms can predict the epicenter and the occurrence time simultaneously. And the prediction accuracy acquired with our model is better than most other prediction strategies.

2. Methodology

2.1. Data acquisition

Global earthquakes with $M \geq 8.0$ over the past 100 years (and some earthquakes with *M* of 6.6-7.9 that have caused significant casualties worldwide; TDEs), as well as triggering earthquakes (TGEs) with $M \geq 4.0$ within 3000 km and 300 days around them, have been summarized (Table S1 of the supplementary materials). The TGEs within 200 km of the epicenter of each TDE are listed in Table S2 (see supplementary materials). Information about epicenters and occurrence times of these earthquakes was acquired from the U. S. Geological Survey (USGS) Web page (earthquake.usgs.gov/earthquakes). The distance from the triggering epicenter to the triggered epicenter was calculated using the GPScalc(sh3) V1.2 software (Elmeligy Abdelhamid et al., 2015). The time interval between TGE and TDE was calculated in Microsoft Excel 2013.

2.2. Data refinement

The data has been refined as follows: If a subsequent earthquake with a smaller magnitude (within one order of magnitude) occurs within a

radius of 50 km after the occurrence of the first TGE, this indicates that the first earthquake activated a seismic structure less than 50 km away. The occurrence of the subsequent earthquake (aftershock) means that tectonic stress was largely released and therefore may not activate other faults at long distances. In this case, we exclude the first earthquake from our analysis.

If the subsequent earthquake with a reduction of more than one order of magnitude occurs within a radius of 50 km after the occurrence of the first TGE, this indicates that the tectonic stress was only partly released, and therefore, it may still activate other faults at long distances. In this case, we do not exclude the first earthquake from our analysis.

The larger the magnitude of the TGE is, the larger the geographic area it can affect, so the greater the distance between the TGE and TDE is, and the longer the time interval between the TGE and TDE is. We roughly analyzed correlations between the magnitude and distance (from TGE to TDE) and between the magnitude and time interval (from TGE to TDE). Then we found that, for TDEs with $M \geq 6.0$, the distances usually range from 300 km to 3000 km; for TDEs with $M \geq 5.7$, the time intervals usually range from 50 days to 300 days. To obtain better regression equations, the data with too low distances (< 300 km for $M \geq 6.0$) or too low time intervals (< 50 d for $M \geq 5.7$) were ruled out [marked with "(L)" and crossed out in Table S1 of the supplementary materials]. Too large time intervals (> 365 days) were also ruled out. The low-magnitude earthquakes were excluded because most small earthquakes with $M < 4.0$ were merely aftershocks of some large-scale earthquakes with $M > 5.0$.

2.3. Correlation and statistical analysis

The correlations between the magnitude and distance (TGE to TDE) and between the magnitude and time interval (TGE to TDE) were calculated. The F-test was performed to analyze all the correlations and to determine whether the data pairs fit the regression model (linear, quadratic, logarithmic, and exponential regressions were tested). The regression equation, the correlation coefficient, and the P-value were obtained by using SPSS v19.0 and Microsoft Excel 2013. The P-value threshold and R^2 threshold for the statistical significance of claims of correlations were 0.05 and 0.5, respectively.

2.4. Prediction method and prediction accuracy estimation

Concentric circles around all the TGEs were drawn with the distances obtained from the regression equations as the radii. In terms of the equation selection, the effect of the first/second or the last TGE may reach large distances, so the maximum distance value obtained from the equations should be selected, and the distance values of the remaining TGEs should be selected to intersect with (be tangent to) it as much as possible. However, in some cases, the distances between TEGs and the TDE were too close (less than 1200 km), the second largest distance or the third largest distance obtained from the equations may be selected. There are multiple intersections for multiple TGEs. The predicted epicenter of TDE should be in the area with the highest degree of overlap.

For each TGE, the calculated time intervals are a range (the left boundary is the minimum value obtained from the equations, and the right boundary is the maximum value obtained from the equations), which can be defined as a time frame. Each TGE has its corresponding time frame (drawn with Microsoft Excel 2013), and the TDE often occurred at the intersection of multiple time frame boundaries. There may be multiple intersections for multiple TGEs. The predicted occurrence time of TDE should be within the time frame intersection with the highest degree of overlap.

3. Results

3.1. Associations between major earthquakes and surrounding earthquakes

Regression analysis revealed that the distances between TGEs and the TDE were concentrated within four bands, which can be described by four quadratic regression equations with R^2 values of > 0.5, although for all the data points only a weak correlation ($R^2 < 0.5$ but $P < 0.01$) was found (Fig. 1a). Interestingly, for all these quadratic equations, the distances reached their maximum values around a magnitude of 6.5. As the magnitude increased further, the distance decreased. They were not linearly correlated.

The time intervals between TGEs and the TDE were linearly and positively correlated with the magnitude. Although some values were too large or too small (for all the data points in Fig. 1b, no significant correlation was found), approximately one-third of the data perfectly fell near three straight lines, which can be described by three linear equations with R^2 values of > 0.95 (Fig. 1b). Because each TDE is associated with multiple TGEs, and one or two of them may have larger effects than the others, and the fact that TDE were too large or too small might be explained.

For the TGEs with magnitudes of 4.3–7.5, the calculated distances based on four quadratic regression equations and the calculated time intervals based on three linear regression equations are summarized in Table S3 of the supplementary materials.

3.2. Validation of the prediction model using historical large-scale earthquakes

Through these regression equations, we have verified 14 earthquakes with magnitudes greater than 6.6. For the M9.0 Kamchatka (Russia) earthquake on Nov. 5, 1952 (Fig. 2a), there were

three TGEs associated with it, and there were two TGEs within 110 km of the TDE's epicenter. Circles centered on the TGEs outside a radius of 200 km are marked in red. Their overlapping regions are marked in pink. The time frames for the TGEs outside a radius of 200 km and the TGEs within 200 km of the TDE's epicenter are denoted by the light-red and light-blue squares, respectively. The purple triangle indicates the occurrence time of the TDE. The blue triangle indicates the occurrence time of the TGE within 200 km from the TDE's epicenter or the middle value in the time frame of the TGE (Fig. 2).

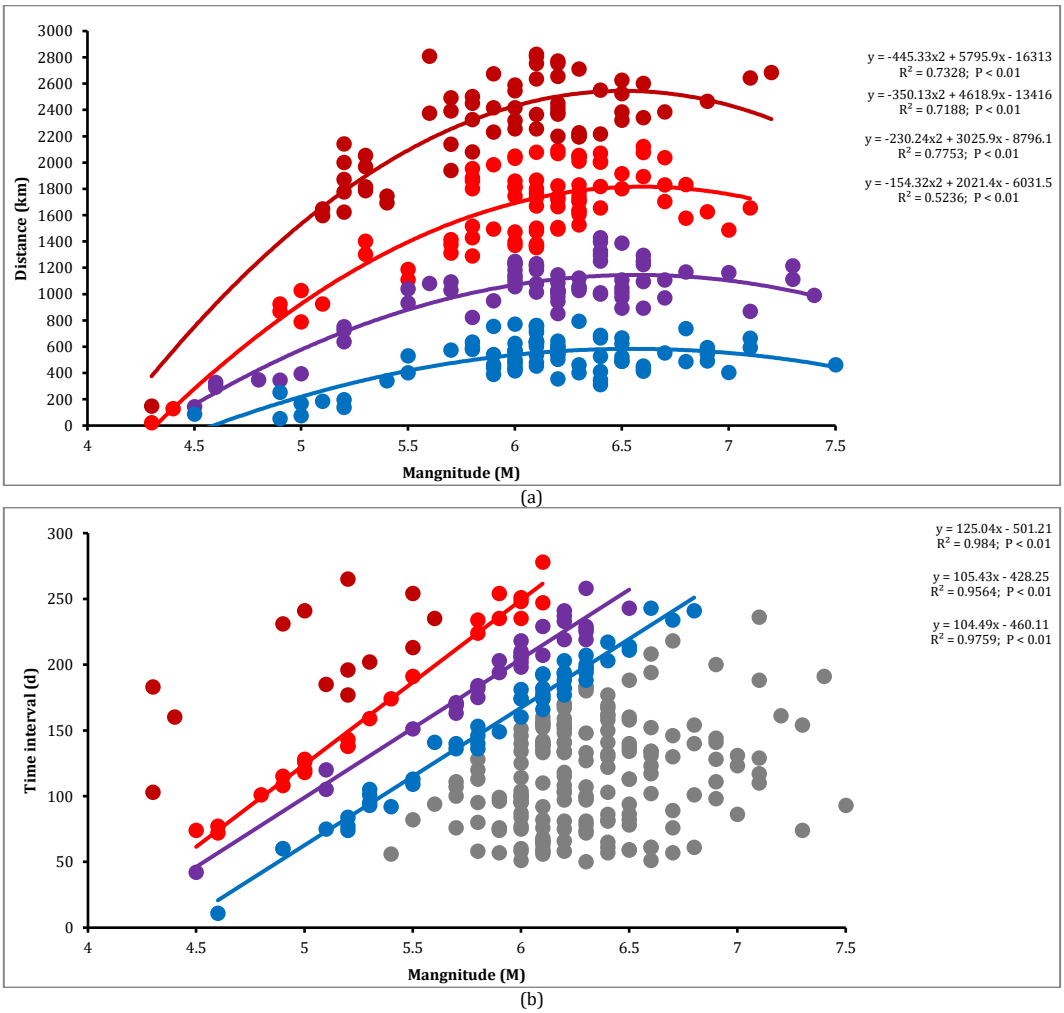

Fig. 1: Regression analysis between magnitude and (a) the distance from triggering earthquakes to triggered earthquakes, and (b) the time interval between TGEs and TDEs

A circle centered on the earliest TGE with a radius equal to the maximum distance obtained from the equations was drawn. Then, circles centered on the other TGEs intersected with it. The predicted epicenter of TDE should be in the intersection area with the highest degree of overlap. The occurrence time of the TDE was 243 days after the earliest TGE, which was exactly the middle value in the time frame of the first *M*6.1 TGE (calculated from the purple equation in Fig. 1b). For the *M*9.5 Chile earthquake on May 23, 1960 (Fig. 2b), a circle centered on the second/last TGE (*M*7.1) with a radius equal to the maximum distance obtained from the equations was drawn. There were also five TGEs within 93 km of the TDE's epicenter. The first *M*8.1 TGE occurred on May 21, 1960. The second TDE occurred 2 days later, and this time was exactly located on the left boundary of the time frame for the *M*6.1 TGE. The *M*9.1 Sumatra (Indonesia) earthquake on Dec. 26, 2004 (Fig. 2c), was associated with five TGEs and five TGEs ≥ 4.5 within 120 km. The location of the TDE was determined by drawing a circle centered on the earliest TGE with a radius equal to the maximum distance. The last TGE was *M*4.9, and the left boundary of its time frame was exactly the time when the TDE occurred. The *M*9.1 Tohoku-Oki (Japan) earthquake on Mar. 11, 2011 (Fig. 2d), was associated with three TGEs outside of 200 km and five TGEs ≥ 5.9 within 74 km. The location of the TDE was determined by drawing a circle with the earliest TGE as the center and with a radius equal to the second largest distance between the other two TGEs. The TGE earthquake happened 2 days after the first *M*7.3 TGE.

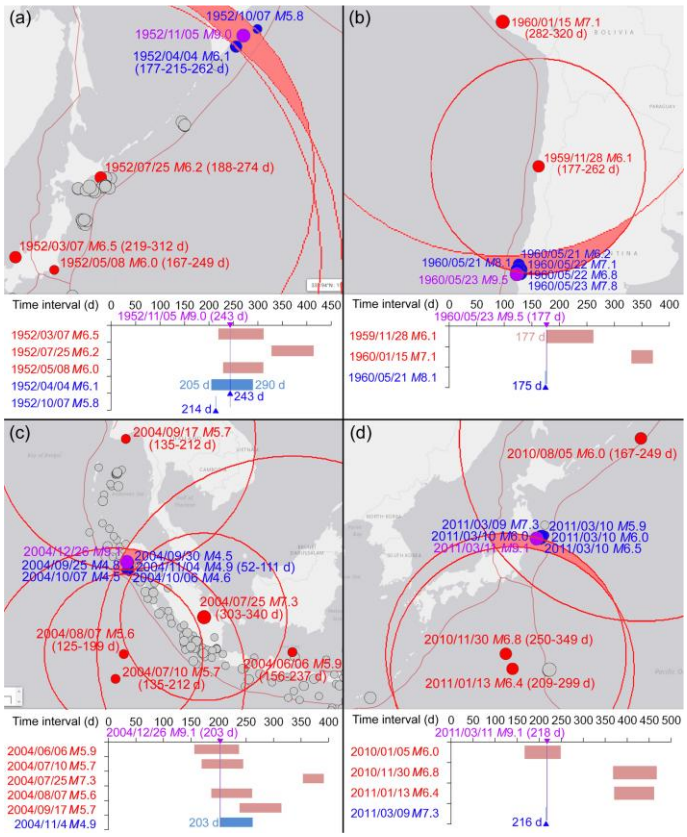

Fig. 2: Prediction and verification of four representative earthquakes with magnitudes M ≥ 9.0: (a) the M9.0 Kamchatka (Russia) earthquake on Nov. 5, 1952; (b) the M9.5 Chile earthquake on May 23, 1960; (c) the M9.1 Sumatra (Indonesia) earthquake on Dec. 26, 2004; and (d) the M9.1 Tohoku-Oki (Japan) earthquake on Mar. 11, 2011

The *M*8.0 Kanto (Japan) Sep. 1, 1923 (Fig. 3a), was associated with four TGEs. The location of the TDE was determined by drawing a circle centered on the earliest TGE with a radius equal to the maximum distance. And the left boundary of its time frame was only one day after the occurrence time of TDE. The *M*7.5 Tangshan (China) earthquake on July 28, 1976 (Fig. 3b), was associated with ten TGEs. The location of the TDE was determined by drawing a circle intersecting the earliest TGE as the center and with a radius equal to the maximum distance between nine cycles of the other nine TGEs. It had three close time frame boundaries of 202, 203, and 204 days (average of 203 days), while the TDE occurred on the 202nd day, with a forecasting error of 1 day. For the *M*7.7 Bhachu (India) earthquake on Jan. 26, 2001 (Fig. 3c), a circle centered on the last TGE with a radius equal to the second largest distance obtained from the equations was drawn. It had a two-timed frame boundaries of 234 and 241 days (average of 237 days), while the TDE occurred on the 235th day, with a forecasting error of 2 days. The *M*8.4 Peru earthquake on Jun. 24, 2001 (Fig. 3d), was associated with four TGEs. A circle with the last TGE as the center and the second largest distance as the radius was drawn. The right boundary of the time frame for the earliest TGE was 237 days, and the left boundary of the time frame for the subsequent TGE was 226 days. Their average value was 232 days. The TDE occurred on the 235th day after the earliest TGE, with a forecasting error of 3 days. The *M*7.0 Haiti earthquake on Jan. 13, 2010 (Fig. 4a), was associated with seven TGEs. The location of the TDE was determined by drawing a circle with the last TGE as the center and with a radius equal to the maximum distance intersected by six cycles of the other six TGEs. The occurrence time of the TDE was 254 days after the earliest TGE, which was one day before the middle value in the time frame of the *M*5.5 TGE on Aug. 15, 2009 (calculated from the purple equation in Fig. 1b). The *M*7.8 Nepal earthquake on Apr. 25, 2015 (Fig. 4b), was associated with four TGEs. A circle with the last (*M*5.3) TGE as the center and the maximum distance as the radius was drawn. The right boundaries of the time frames for two TGEs were 261 and 268 days, while the left boundary of the time frame of another TGE was 258 days. The average value was 262 days. The TDE occurred on the 265th day after the earliest TGE, with a forecasting error of 3 days. The *M*7.8 Turkey earthquake on Feb. 6, 2023 (Fig. 4c), was associated with three TGEs.

A circle with the last TGE as the center and the maximum distance as the radius was drawn. There were also five TGEs ≥ 4.0 within 82 km of the TDE's epicenter. The last TGE within 200 km occurred 238 days after the earliest TGE, and the TDE occurred on the 241st day. The recent *M*7.7 Myanmar earthquake on Mar. 28, 2025 (Fig. 4d), was associated with three TGEs. A circle with the last TGE as the center and the third distance as the radius was drawn. The left boundary of the last TGE was 113 days, and the TDE occurred on the 114th day after the last TGE, with a forecasting error of 1 day.

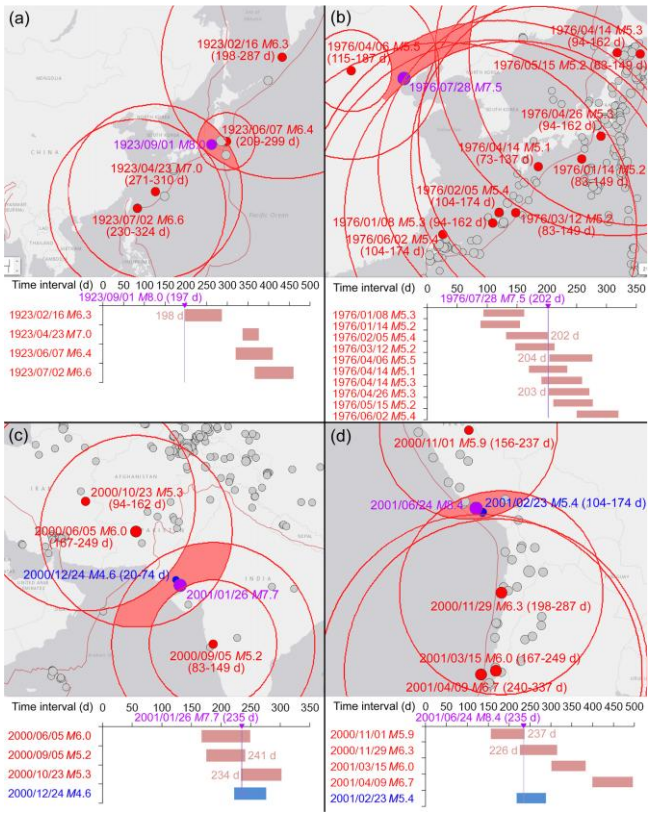

Fig. 3: Prediction and verification of four representative earthquakes with magnitudes M 7.5–8.4 from 1923 to 2002: (a) the M8.0 Kanto (Japan) earthquake on Sep. 1, 1923; (b) the M7.5 Tangshan (China) earthquake on July 28, 1976; (c) the M7.7 Bhachu (India) earthquake on Jan. 26, 2001; and (d) the M8.4 Peru earthquake on Jun. 24, 2001

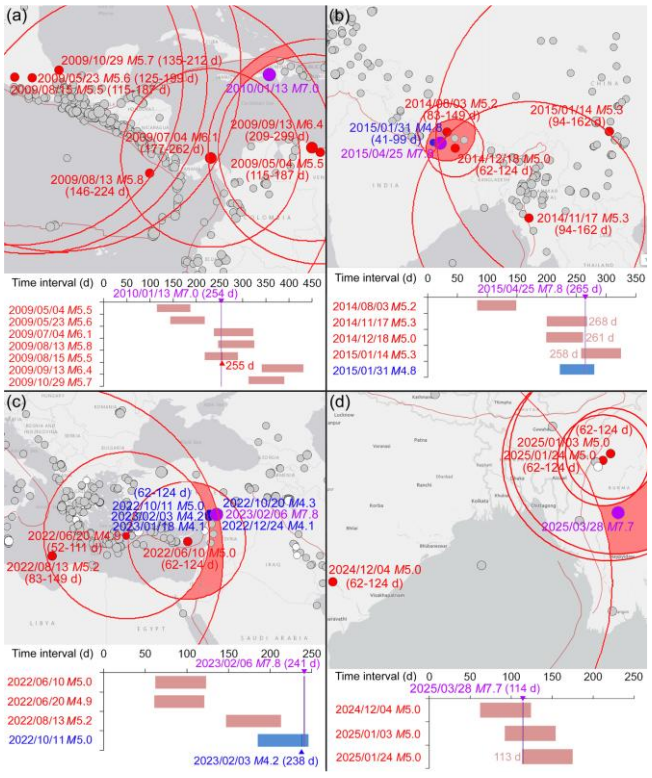

Fig. 4: Prediction and verification of four representative earthquakes with magnitudes M 7.0–7.8 from 2010 to 2025: (a) the M7.0 Haiti earthquake on Jan. 13, 2010; (b) the M7.8 Nepal earthquake on Apr. 25, 2015; (c) the M7.8 Turkey earthquake on Feb. 6, 2023; and (d) the M7.7 Myanmar earthquake on Mar. 28, 2025

In Sichuan province, China, the *M*7.9 Wenchuan (China) earthquake on May 12, 2008 (Fig. 5a), was associated with three TGEs. A circle with the earliest TGE as the center and the second largest distance as the radius was drawn. Both the right boundary of the *M*4.8 TGE and the left boundary of the *M*5.1 TGE were at the 113th day, and the TDE occurred on the 115th day after the earliest TGE, with a forecasting error of 2 days. The *M*6.6 Lushan (China) earthquake on Apr. 20, 2013, had two-time frame boundaries of

93 and 103 days (average of 98 days; Fig. 5b), while the TDE occurred on the 101st day, with a forecasting error of 3 days. The *M*6.6 Luding (China) earthquake on Sept. 5, 2022, had two-time frame boundaries of 157 and 163 days (average of 160 days; Fig. 5c), while the TDE occurred on the 160th day, without a forecasting error.

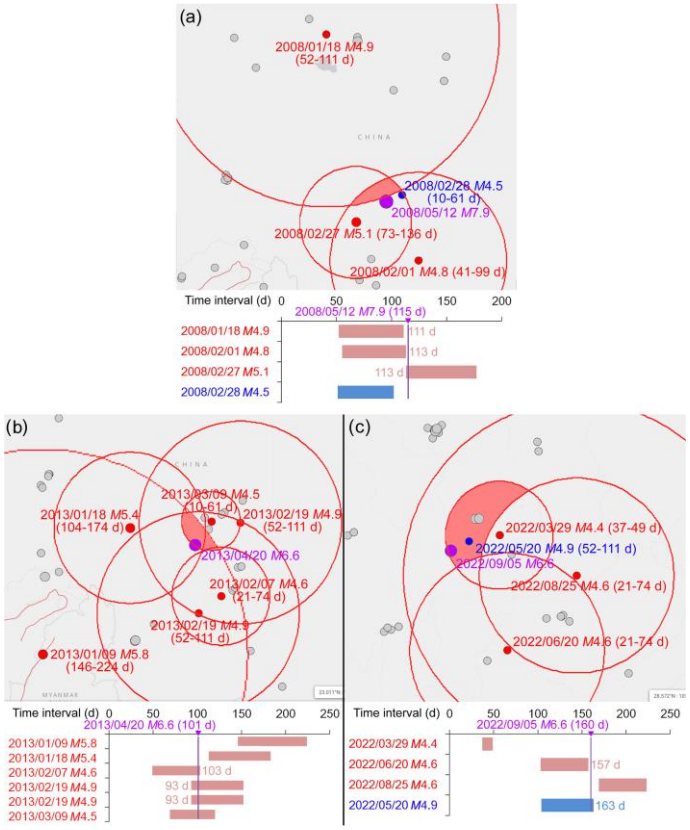

Fig. 5: Prediction and verification of major earthquakes in Sichuan, China: (a) the M7.9 Wenchuan earthquake on May 12, 2008; (b) the M6.6 Lushan earthquake on Apr. 20, 2013; and (c) the M6.6 Luding earthquake on Sep. 5, 2022

3.3. Prediction accuracy

In the past 100 years, earthquakes of $M \geq 9.0$ and earthquakes that have caused significant casualties (e.g. the *M*8.0 Kanto earthquake in 1923, the *M*9.5 Chile earthquake in 1960, the *M*7.5 Tangshan earthquake in 1976, the *M*9.1 Sumatra earthquake in 2004, the *M*7.9 Wenchuan earthquake in 2008, the *M*7.0 Haiti earthquake in 2010, the *M*9.1 Tohoku-Oki earthquake in 2011, and the *M*7.8 Turkey earthquake in 2023) all met our model (Table 1).

Besides the above earthquakes, we predict a future earthquake in Japan based on this model. The right boundary of the M6.0 TGE (Jan. 21) is very close to the left boundary of the M6.1 TGE (Apr. 2), and the TDE may occur on those two days. Alternatively, the right boundary of the M6.1 TGE (Apr. 2) is very close to the middle value of the M6.0 TGE (May 31), and the TDE may occur on those two days. The purple dot indicates the joint of the two main fault zones in Japan, which is very close to the intersection area with the highest degree of overlap. Thus, the purple dot might be the future epicenter of TDE. Considering that the major earthquakes in recent decades have all occurred on the west side of the main fault zone in Japan, the actual epicenter may be located about 100 km west of the purple dot (Fig. 6). In summary, the location of the TDE can be determined by multiple TGEs, with the distance calculated based on four quadratic regression equations. TDEs often occurred at the intersection of multiple time frame boundaries or 1–3 days after the first or last TGE within 200 km. Based on this method, we were able to predict the epicenter locations of TDEs with a success rate of 89% (77/87) and the occurrence times of TDEs with a success rate of 63% (55/87) (Table S4 of the supplementary materials). It can be summarized from Table 1 that the forecasting error range for large-scale earthquakes in densely populated areas was within 100 km and 3 days. However, the epicenter may not be a reliable marker of the spatial localization of large events. For example, the centroid of released deformation of the *M*9.1 Sumatra earthquake on Dec. 26, 2004, was located at least 200 km north of the seismological epicenter (Vigny et al., 2005). Nevertheless, the centroid data are not always available. The accurate forecast error of the distance needs further investigation.

4. Discussion

The lithosphere of the Earth is not completely rigid, and the tectonic plate interaction is affected by the characteristics of the plates, the angle of subduction, and the geological conditions (Nur and Mavko, 1974; Peltzer et al., 1999; Delorey et al., 2015).

Table 1: Success rate of the proposed forecasting model for large-scale earthquakes in densely populated regions

Time	*M*	Location	Prediction of the epicenter by which TGEs, with which distance (km) (actual distance; km)	Predicted time (d) after the first TGE (actual time)
1952/11/5	9.0	52.623°N 159.779°E (Kamchatka, Russia)	First TGE with max dis. of 2545 (2626)	243 (243)
1964/3/28	9.2	60.908°N 147.339°W (Alaska, USA)	First TGE with max dis. of 2322 (2326) Second TGE with max dis. of 2255 (2391)	183 (184)
1923/9/1	8.0	35.274°N 139.344°E (Japan)	Last TGE with second dis. of 1647 (1565)	198 (197)
1941/11/19	8.0	32.129°N 131.944°E (Japan)	First TGE with third dis. of 1114 (1031) Second TGE with second dis. of 1786 (1702)	204 (203)
1946/12/21	8.3	33.123°N 135.905°E (Japan)	First TGE with second dis. of 1536 (1471)	204 (202)
1952/3/4	8.1	42.084°N 143.899°E (Japan)	First TGE with second dis. of 1728 (1653)	239 (236)
2011/3/11	9.1	38.297°N 142.373°E (Japan)	Second TGE with third dis. of 1134 (1167)	217-219 (218)
2008/5/12	7.9	31.002°N 103.322°E (Sichuan, China)	First TGE with second dis. of 810 (867)	113 (115)
2013/4/20	6.6	30.308°N 102.888°E (Sichuan, China)	First TGE with third dis. of 1009 (961)	93-103 (101)
2022/9/5	6.6	29.679°N 102.236°E (Sichuan, China)	Last TGE with second dis. of 422 (326)	157-163 (160)
1976/7/28	7.5	39.570°N 117.978°E (Tangshan, China)	First TGE with max dis. of 1784 (1786)	202-204 (202)
2001/1/26	7.7	23.419°N 70.232°E (India)	Last TGE with second dis. of 1316 (1400)	234-241 (235)
2005/10/8	7.6	34.539°N 73.588°E (Pakistan)	First TGE with second dis. of 1034 (935)	168-203 (185)
2023/2/6	7.8	37.174°N 37.032°E (Turkey)	Last TGE with max dis. of 1784 (1776)	238 (241)
2015/4/25	7.8	28.231°N 84.731°E (Nepal)	Last TGE with max dis. of 1896 (1814)	258-268 (265)
2004/12/26	9.1	3.295°N 95.982°E (Indonesia)	First TGE with max dis. of 2322 (2230)	203 (203)
2012/4/11	8.6	2.327°N 93.063°E (Indonesia)	Second TGE with max dis. of 2471 (2505)	214-228 (218)
1985/9/19	8.0	18.190°N 102.533°W (Mexico)	First TGE with third dis. of 1009 (1092)	173 (171)
2017/9/8	8.2	15.022°N 93.899°W (Mexico)	Second TGE with max dis. of 2178 (2138)	224-244 (234)
2010/1/13	7.0	18.443°N 72.571°W (Haiti)	Last TGE with max dis. of 2255 (2292)	255 (254)
1960/5/23	9.5	38.143°S 73.407°W (Chile)	First TGE with third dis. of 1095 (1077)	176-178 (177)
1970/8/1	8.0	1.597°S 72.532°W (Peru)	First TGE with max dis. of 2431 (2416) Last TGE with max dis. of 2541 (2600)	205 (206)
1985/3/4	8.0	33.135°S 71.871°W (Chile)	First TGE with third dis. of 1114 (1144)	135-137 (134)
2001/6/24	8.4	16.265°S 73.641°W (Peru)	Last TGE with second dis. of 1813 (1829)	226-237 (235)
2010/2/27	8.8	36.122°S 72.898°W (Chile)	First TGE with max dis. of 2381 (2451) Second TGE with max dis. of 2381 (2415)	169-184 (175)
2014/4/2	8.2	19.610°S 70.769°W (Chile)	Last TGE with second dis. of 1804 (1889)	233-235 (233)

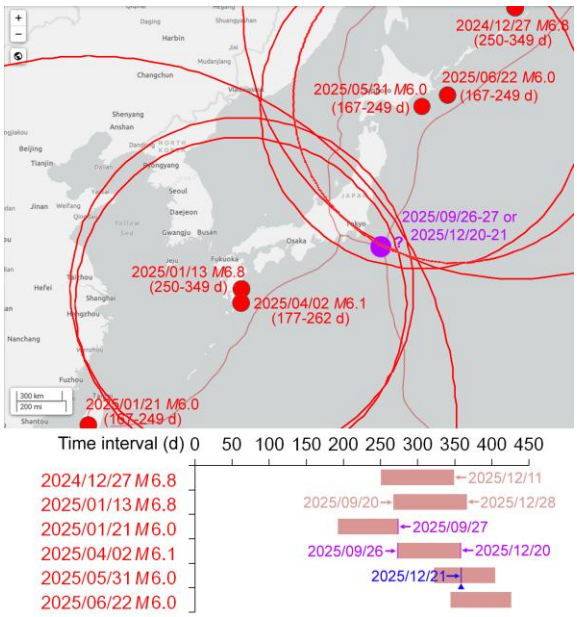

Fig. 6: Predicted location and possible occurrence time of a future earthquake in Japan based on the proposed regression model and the spatial overlap of calculated epicentral distances

Rocks initially respond to these forces by deforming elastically. Then rocks can get stretched and form cracks or fractures along fault lines in regions where they are subjected to severe stress. These flaws are areas of vulnerability where the built-up stress can be discharged. When the cumulative tension on the rocks reaches their elastic limit, they can no longer deform elastically and instead fracture and slide along fault lines. It can result in the abrupt release of energy in the form of seismic waves, which causes an earthquake. Rapid seismic wave creation is caused by this quick release of accumulated stress, and these waves travel throughout the earth in all directions (Nur and Mavko, 1974; Peltzer et al., 1999; Delorey et al., 2015). Our algorithm fits the theory of elasticity, which states that the flaws are relatively elastic. The multiple TGEs may generate combined effects on vulnerable rock formation in the fault line, so that the stress may surpass the threshold, and the TDE

would be triggered. The plates are like teeterboards of rocks floating on the mantle. The larger the magnitude of the TGE is, the larger the plate it can shake, so the greater the distance between the TGE and TDE is. In addition, the larger the magnitude of the TGE is, the greater the shift it causes on the other side of the plate boundary, and therefore, the longer the interval between the TGE and TDE is.

Many articles suggested that faulting is a non-linear process which is very sensitive to unmeasurable fine details of the state of the earth crust in a large volume, not merely in the immediate vicinity of the hypocenter (Huang et al., 2017; Lambert et al., 2021; Nandan et al., 2022). Here, we found that the distances between TGEs and the TDE were non-linearly correlated with the magnitude, which may be described by four quadratic regression equations.

Thus, there is a chance that any small-scale earthquake will eventually grow into a large event. But not all large earthquakes trigger other earthquakes (Huang et al., 2017). A recent article showed the complexity of forecasting and specified that forecasting should model putative time variations of regional or local strain fields and other related fields that might be associated with seismicity (Nandan et al., 2022). To precisely predict the time of an earthquake, we need to know the exact stresses applied to the fault throughout its sliding history. The static and transient deformation changes may hasten the occurrence of future earthquakes (Lambert et al., 2021). The spatio-temporal distribution of seismicity can change due to the activation of previously inactive faults. By a mechanism known as dynamic stress transfer/triggering, earthquakes, especially big ones, can occasionally set off smaller, farther-off earthquakes. This indicates that a new earthquake may be caused by the energy of the seismic wave that passes through, usually in areas that are already sensitive and prone to frequent earthquakes (e.g., volcanic zones). However, not every significant earthquake sets off another one (Huang et al., 2017; Lambert et al., 2021; Nandan et al., 2022). Consistent with this viewpoint, it is not always possible to find multiple precursor earthquakes before every large-scale earthquake in our analysis. Only 89% of large-scale earthquake epicenters and 63% of occurrence times can be accurately predicted by our model.

The georesistivity decreases sharply within a time frame of several hours to 2 days before the earthquake, and when it drops to an extremum, a large earthquake will occur in 6–42 hours. Qian et al. (2009) predicted the Wenchuan (China) *M*7.9 earthquake successfully by using this model. However, they did not predict the location of the epicenter. The maximum thermal infrared anomalies appear at 1 day to 6 months before large-scale earthquakes of $M \geq 7.0$ (Wei et al., 2013). While pre-seismic anomalies from multi-channel infrared remote sensing images may predict large earthquakes within 200 km and one month (Yue et al., 2022). Akhoondzadeh and Marchetti (2022) developed a Mamdani fuzzy inference system (FIS) with the data of anomalies to predict earthquake magnitude. They found that the highest value of anomalies was often found about one month before the earthquake. Neural network algorithms are usually used to forecast the maximum magnitude of future events in a certain region. However, the time frame ranges from one week to one year, depending on the geological structure. For example, an LSTM neural network can forecast the maximum magnitudes of earthquakes in the Yunnan–Sichuan region in China (Wang et al., 2023). While for earthquake-prone countries, such as Iran, the machine learning algorithms by the methods of Support Vector Machine (SVM) may predict the magnitude of the biggest future earthquake in the next week (Yousefzadeh et al., 2021). The slope unit-based logistic regression and geospatial statistics have been used for assessment of earthquake-induced landslide inventories, but not for future earthquake prediction (Pokharel et al., 2021). Therefore, the prediction accuracy of 100 km and 3 days acquired with our model is better than most current baseline models and publicly available benchmark datasets. Another merit of our prediction method is that it can predict the epicenter and the occurrence time simultaneously. However, our algorithms cannot forecast the magnitude, which could just be compensated for by the machine learning methods.

The forecasting error may be a little large for some earthquakes. However, if combined with the analysis of local earthquake zones, TDEs may be located more accurately (within 20 km), such as the *M*6.6 Luding (China) earthquake (Fig. 5c), the epicenter of which was successfully forecasted in our previous study. Briefly, the Longmen Mountain fault zone includes three parallel fault zones. In 2008 and 2013, two earthquakes of $M \geq 7.0$ occurred in the middle zone and the east zone, respectively. Therefore, the accumulated stress energy has been released. And the northeast zone was relatively fragile (Chen et al., 2008), where no large-scale earthquake has occurred since 1786, and the stress has been accumulated for a long time (Chen et al., 2008; Hubbard and Shaw, 2009). This area is the joint of the west Longmen mountain fault zone, the Xianshui river fault zone, and the An'ning river fault zone. Similarly, stress accumulation and the seismic migration near the Tangshan (China) fault (Shao et al., 2021), the north Anatolian (Turkey) fault (Steinmann et al., 2022), and the Japan Trench fault (Kodaira et al., 2021) have also been analyzed.

For the countries in the Circum-Pacific seismic belt (such as Indonesia, Japan, and Chile), before each large earthquake, several precursor earthquakes within 200 km of the epicenter of the TDE were usually found. TDEs often occurred at 1–3 days after the first or the last TGE within 200 km. This fact may help us to improve the prediction accuracy, especially if region-specific machine learning algorithms were combined. The mechanisms of earthquakes are complex, and

therefore most predictions (or some simple correlations) are "still the stuff of science fiction." Though good correlations have been acquired in this study by some selections on the data, for all the data points, only a weak or no correlation was found. So, a data processing mechanism is required in conditions of a deficiency of statistical information. Analyzing laboratory and field data with artificial intelligence and other related algorithms may maximize the information retrieved from the data and improve the prediction power that can be acquired from different observations. Recently, two articles present an advance in methods of achieving a high level of serviceability and reliability of the earthquake correlation system (Rundle et al., 2021; Tehseen et al., 2021). Bao et al. (2021) proposed a deep convolutional neural network (CNN; Jozinović et al., 2020) and designed a three-dimensional feature map that could be adopted to solve the problems of earthquake magnitude classification by incorporating high-dimensional information with the shallow features. Furthermore, noise simulation technology and synthetic minority over-sampling techniques (SMOTE; Xu et al., 2019; Banerjee et al., 2020) could be adopted to overcome the imbalance problems of the seismic data (Bao et al., 2021). More mathematical analysis on anomalies and the correlations among earthquakes is needed in the future.

Considering that only 63%–88% of large-scale earthquakes can be accurately predicted by our algorithms, and there are certain errors in the time and location ranges, we should not issue evacuation warnings to the public based on this prediction model. But high-risk populations (such as those living in dangerous buildings) and vulnerable facilities (such as nuclear power plants) should make some preparation beforehand, and crowded places (such as tourist attractions) should be closed in the critical period.

5. Conclusions

In this study, we first reported the quantitative associations between precursor earthquakes (triggering earthquakes; TGEs) and triggered earthquake (TDE). Regression analysis revealed that the distances between TGEs and the TDE were concentrated within four bands, which can be described by four quadratic regression equations with R^2 values of > 0.5. And the time intervals between TGEs and TDE were linearly and positively correlated with the magnitude, which can be described by three linear equations with R^2 values of > 0.95. Based on the regression equations, a prediction method was proposed. Then we retrospect 86 large earthquakes ($M \geq 6.6$) over the past 100 years to testify to the adequacy of our model for practical earthquake forecasting. And we found that, although we are only able to predict only 63%–88% of large-scale earthquakes, earthquakes of $M \geq 9.0$ and earthquakes that have caused significant casualties all met our model with a prediction accuracy of 100 km and 3 days.

However, our algorithms cannot forecast the magnitude. And the region-specific earthquake triggering mechanisms are not included in our model. We thus should consider many other characteristics to obtain an effective prediction, for instance, the TIR radiation emitting or reference to the machine learning prediction results.

List of abbreviations

CH_4	Methane
CNN	Convolutional neural network
CO_2	Carbon dioxide
D	Day
d	Day
dis	Distance
DNN	Deep neural network
DT	Decision tree
FIS	Fuzzy inference system
GRU	Gated recurrent unit (gated recurrent network)
HT	Harmonic oscillation wave driven by tidal force
InSAR	Interferometric synthetic aperture radar
LSTM	Long short-term memory neural network
M	Magnitude
P-wave	Pressure wave
RTL	Region–time–length algorithm
R^2	Coefficient of determination
S-wave	Shear wave
SMOTE	Synthetic minority over-sampling technique
SNN	Shallow neural network
SVM	Support vector machine
TDE	Triggered earthquake
TEC	Total electron content
TGE	Triggering earthquake
TIR	Thermal infrared radiation
USGS	United States Geological Survey

Funding

This work was supported by the Sichuan Province Youth Science and Technology Innovation Team (20CXTD0062) to SY and the Applied Basic Research Program of Sichuan Province (2020YJ0410) to ZWZ.

Compliance with ethical standards

Conflict of interest

The author(s) declared no potential conflicts of interest with respect to the research, authorship, and/or publication of this article.

References

Akhoondzadeh M and Marchetti D (2022). Developing a fuzzy inference system based on multi-sensor data to predict powerful earthquake parameters. Remote Sensing, 14(13): 3203. https://doi.org/10.3390/rs14133203

Banerjee A, Bhattacharjee M, Ghosh K, and Chatterjee S (2020). Synthetic minority oversampling in addressing imbalanced sarcasm detection in social media. Multimedia Tools and Applications, 79: 35995–36031. https://doi.org/10.1007/s11042-020-09138-4

Bao Z, Zhao J, Huang P, Yong S, and Wang X (2021). A deep learning-based electromagnetic signal for earthquake magnitude prediction. Sensors, 21(13): 4434. https://doi.org/10.3390/s21134434 **PMid:34203508 PMCid:PMC8272143**

Berhich A, Belouadha FZ, and Kabbaj MI (2022). A location-dependent earthquake prediction using recurrent neural network algorithms. Soil Dynamics and Earthquake Engineering, 161: 107389. https://doi.org/10.1016/j.soildyn.2022.107389

Beroza GC, Segou M, and Mousavi SM (2021). Machine learning and earthquake forecasting—next steps. Nature Communications, 12: 4761. https://doi.org/10.1038/s41467-021-24952-6 **PMid:34362887 PMCid:PMC8346575**

Bletery Q and Nocquet JM (2023). The precursory phase of large earthquakes. Science, 381(6655): 297–301. https://doi.org/10.1126/science.adg2565 **PMid:37471540**

Chen Y, Li L, Li J, and Li G (2008). Wenchuan earthquake: Way of thinking is changed. Episodes, 31(4): 374–377. https://doi.org/10.18814/epiiugs/2008/v31i4/001

Cisternas M, Atwater BF, Torrejón F et al. (2005). Predecessors of the giant 1960 Chile earthquake. Nature, 437: 404–407. https://doi.org/10.1038/nature03943 **PMid:16163355**

Cyranoski D (2004). Earthquake prediction: A seismic shift in thinking. Nature, 431: 1032. https://doi.org/10.1038/4311032a **PMid:15510118**

Dascher-Cousineau K, Shchur O, Brodsky EE, and Günnemann S (2023). Using deep learning for flexible and scalable earthquake forecasting. Geophysical Research Letters, 50(17): e2023GL103909. https://doi.org/10.1029/2023GL103909

Delorey AA, Chao K, Obara K, and Johnson PA (2015). Cascading elastic perturbation in Japan due to the 2012 Mw 8.6 Indian Ocean earthquake. Science Advances, 1: e1500468. https://doi.org/10.1126/sciadv.1500468 **PMid:26601289 PMCid:PMC4646803**

Denolle MA, Dunham EM, Prieto GA, and Beroza GC (2014). Strong ground motion prediction using virtual earthquakes. Science, 343(6169): 399–403. https://doi.org/10.1126/science.1245678 **PMid:24458636**

Eleftheriou A, Filizzola C, Genzano N, Lacava T, Lisi M, Pergola N, Scaffidi I, and Tramutoli V (2016). Long-term RST analysis of anomalous TIR sequences in relation with earthquakes occurred in Greece in the period 2004–2013. Pure and Applied Geophysics, 173: 285–303. https://doi.org/10.1007/s00024-015-1116-8

Elmeligy Abdelhamid SH, Kuhlman CJ, Marathe MV, Mortveit HS, and Ravi SS (2015). GDSCalc: A web-based application for evaluating discrete graph dynamical systems. PLOS ONE, 10(8): e0133660. https://doi.org/10.1371/journal.pone.0133660 **PMid:26263006 PMCid:PMC4532456**

Friedmann H (2012). Radon in earthquake prediction research. Radiation Protection Dosimetry, 149(2): 177–184. https://doi.org/10.1093/rpd/ncr229 **PMid:21669940**

Gambino S, Laudani A, and Mangiagli S (2014). Seismicity pattern changes before the M = 4.8 Aeolian Archipelago (Italy) earthquake of August 16, 2010. The Scientific World Journal, 2014: 531212. https://doi.org/10.1155/2014/531212 **PMid:24511288 PMCid:PMC3910363**

Hall S (2023). What Turkey's earthquake tells us about the science of seismic forecasting. Nature, 615: 388–389. https://doi.org/10.1038/d41586-023-00685-y **PMid:36878981**

Han R, Cai M, Chen T, Yang T, Xu L, Shen X, Li J, and Liu J (2022). Preliminary study on the generating mechanism of the atmospheric vertical electric field before earthquakes. Applied Sciences, 12(14): 6896. https://doi.org/10.3390/app12146896

Herrera VMV, Rossello EA, Orgeira MJ et al. (2022). Long-term forecasting of strong earthquakes in North America, South America, Japan, Southern China and Northern India with machine learning. Frontiers in Earth Science, 10: 905792. https://doi.org/10.3389/feart.2022.905792

Huang F, Li M, Ma Y, Han Y, Tian L, Luan G, and Jin S (2017). Studies on earthquake precursors in China: A review for recent 50 years. Geodesy and Geodynamics, 8(1): 1–12. https://doi.org/10.1016/j.geog.2016.12.002

Hubbard J and Shaw JH (2009). Uplift of the Longmen Shan and Tibetan plateau, and the 2008 Wenchuan (M = 7.9) earthquake. Nature, 458: 194–197. https://doi.org/10.1038/nature07837 **PMid:19279635**

Jozinović D, Lomax A, and Stajduhar I (2020). Rapid prediction of earthquake ground shaking intensity using raw waveform data and a convolutional neural network. Geophysical Journal International, 222(2): 1379–1389. https://doi.org/10.1093/gji/ggaa233

Kerr RA (2011). Earthquake prediction: A quake may have hinted that it was on the way. Science, 331(6019): 836. https://doi.org/10.1126/science.331.6019.836 **PMid:21330502**

Klyuev RV, Morgoev ID, Morgoeva AD, Gavrina OA, and Martyushev NV (2022). Methods of forecasting electric energy consumption: A literature review. Energies, 15(23): 8919. https://doi.org/10.3390/en15238919

Kodaira S, Iinuma T, and Imai K (2021). Investigating a tsunamigenic megathrust earthquake in the Japan Trench. Science, 371(6534): eabe1169. https://doi.org/10.1126/science.abe1169 **PMid:33707238**

Lambert V, Lapusta N, and Faulkner D (2021). Scale dependence of earthquake rupture prestress in models with enhanced weakening: Implications for event statistics and inferences of fault stress. Journal of Geophysical Research: Solid Earth, 126(10): e2021JB021886. https://doi.org/10.1029/2021JB021886

Lin JW (2013). Ionospheric anomalies related to the (M = 7.3), August 27, 2012, Puerto earthquake, (M = 6.8), August 30, 2012 Jan Mayen Island earthquake, and (M = 7.6), August 31, 2012, Philippines earthquake: Two-dimensional principal component analysis. The Scientific World Journal, 2013: 271513. https://doi.org/10.1155/2013/271513 **PMid:23844386 PMCid:PMC3690271**

Liu C, Lay T, Wang R et al. (2023a). Complex multi-fault rupture and triggering during the 2023 earthquake doublet in southeastern Türkiye. Nature Communications, 14: 5564. https://doi.org/10.1038/s41467-023-41404-5 **PMid:37689816 PMCid:PMC10492857**

Liu J, Zhang T, Gao CL, and Wang PX (2023b). Forecasting earthquake magnitude and epicenter by incorporating spatiotemporal priors into deep neural networks. IEEE Transactions on Geoscience and Remote Sensing, 61: 5911413. https://doi.org/10.1109/TGRS.2023.3281784

Moro M, Saroli M, Stramondo S, Bignami C, Albano M, Cinti FR, and Falcucci E (2017). New insights into earthquake precursors from InSAR. Scientific Reports, 7(1): 12035. https://doi.org/10.1038/s41598-017-12058-3 **PMid:28931843 PMCid:PMC5607348**

Mousavi SM and Beroza GC (2022). Deep-learning seismology. Science, 377(6607): eabm4470. https://doi.org/10.1126/science.abm4470 **PMid:35951699**

Mousavi SM and Beroza GC (2023). Machine learning in earthquake seismology. Annual Review of Earth and Planetary Sciences, 51: 105–129. https://doi.org/10.1146/annurev-earth-071822-100323

Nandan S, Ouillon G, and Sornette D (2022). Are large earthquakes preferentially triggered by other large events? Journal of Geophysical Research: Solid Earth, 127(8): e2022JB024380. https://doi.org/10.1029/2022JB024380

Nur A and Mavko G (1974). Postseismic viscoelastic rebound. Science, 183: 204–206. https://doi.org/10.1126/science.183.4121.204 **PMid:17777265**

Parsons T, Segou M, and Marzocchi W (2014). The global aftershock zone. Tectonophysics, 618: 1–34. https://doi.org/10.1016/j.tecto.2014.01.038

Peltzer G, Crampé F, and King G (1999). Evidence of nonlinear elasticity of the crust from the Mw7.6 Manyi (Tibet) earthquake. Science, 286(5438): 272–276. https://doi.org/10.1126/science.286.5438.272 **PMid:10514367**

Pokharel B, Alvioli M, and Lim S (2021). Assessment of earthquake-induced landslide inventories and susceptibility maps using slope unit-based logistic regression and geospatial statistics. Scientific Reports, 11(1): 21333. https://doi.org/10.1038/s41598-021-00780-y **PMid:34716368 PMCid:PMC8556321**

Qian FY, Zhao BR, Qian W, Zhao J, and He SG (2009). Impending HRT wave precursors to the Wenchuan Ms8.0 earthquake and methods of earthquake impending prediction by using HRT wave. Science in China Series D: Earth Sciences, 52: 1572–1584. https://doi.org/10.1007/s11430-009-0124-x

Rundle JB, Stein S, Donnellan A, Turcotte DL, Klein W, and Saylor C (2021). The complex dynamics of earthquake fault systems: New approaches to forecasting and nowcasting of earthquakes. Reports on Progress in Physics, 84: 076801. https://doi.org/10.1088/1361-6633/abf893 **PMid:33857928 PMCid:PMC9787018**

Rundle JB, Tiampo KF, Klein W, and Martins JSS (2002). Self-organization in leaky threshold systems: The influence of near-mean field dynamics and its implications for earthquakes, neurobiology, and forecasting. Proceedings of the National Academy of Sciences of the United States of America, 99(1): 2514–2521. https://doi.org/10.1073/pnas.012581899 **PMid:11875204 PMCid:PMC128570**

Shao B, Hou G, and Shen J (2021). Inter-episodes earthquake migration in the Bohai-Zhangjiakou Fault Zone, North China: Insights from numerical modeling. PLOS ONE, 16(5): e0251606. https://doi.org/10.1371/journal.pone.0251606 **PMid:34010347 PMCid:PMC8133458**

Steinmann R, Seydoux L, Beaucé É, and Campillo M (2022). Hierarchical exploration of continuous seismograms with unsupervised learning. Journal of Geophysical Research: Solid Earth, 127(1): e2021JB022455. https://doi.org/10.1029/2021JB022455 **PMid:35864916 PMCid:PMC9285886**

Tehseen R, Farooq MS, and Abid A (2021). A framework for the prediction of earthquake using federated learning. PeerJ Computer Science, 7: e540. https://doi.org/10.7717/peerj-cs.540 **PMid:34141879 PMCid:PMC8176529**

Tramutoli V, Aliano C, Corrado R, Filizzola C, Genzano N, Lisi M, Martinelli G, and Pergola N (2013). On the possible origin of thermal infrared radiation (TIR) anomalies in earthquake-prone areas observed using robust satellite techniques (RST). Chemical Geology, 339: 157–168. https://doi.org/10.1016/j.chemgeo.2012.10.042

Velasco AA, Hernandez S, Parsons T, and Pankow K (2008). Global ubiquity of dynamic earthquake triggering. Nature Geoscience, 1: 375–379. https://doi.org/10.1038/ngeo204

Vigny C, Simons WJ F, Abu S, Bamphenyu R, Satirapod C, Choosakul N, Subarya C, Socquet A, Omar K, Abidin HZ, and Ambrosius BAC (2005). Insight into the 2004 Sumatra-Andaman earthquake from GPS measurements in Southeast Asia. Nature, 436: 201–206. https://doi.org/10.1038/nature03937 **PMid:16015320**

Wang X, Zhong Z, Yao Y, Li Z, Zhou S, and Zhang Y (2023). Small earthquakes can help predict large earthquakes: A machine learning perspective. Applied Sciences, 13(11): 6424. https://doi.org/10.3390/app13116424

Wei C, Zhang Y, Guo X, Hui S, Qin M, and Ma W (2013). Thermal infrared anomalies of several strong earthquakes. The Scientific World Journal, 2013: 208407. https://doi.org/10.1155/2013/208407 **PMid:24222728 PMCid:PMC3809928**

Xu XL, Chen W, and Sun YF (2019). Over-sampling algorithm for imbalanced data classification. Journal of Systems Engineering and Electronics, 30(6): 1182–1191. https://doi.org/10.21629/JSEE.2019.06.12

Yousefzadeh M, Hosseini SA, and Farnaghi M (2021). Spatiotemporally explicit earthquake prediction using deep neural network. Soil Dynamics and Earthquake Engineering, 144: 106663. https://doi.org/10.1016/j.soildyn.2021.106663

Yue Y, Chen F, and Chen G (2022). Statistical and comparative analysis of multi-channel infrared anomalies before earthquakes in China and the surrounding area. Applied Sciences, 12(16): 7958. https://doi.org/10.3390/app12167958

Zhang M, Liu M, Feng T, Wang RJ, and Zhu WQ (2022). LOC-FLOW: An end-to-end machine learning-based high-precision earthquake location workflow. Seismological Research Letters, 93(5): 2426–2438. https://doi.org/10.1785/0220220019